J. Biochem. **133**, 817–823 (2003)
DOI: 10.1093/jb/mvg104

Crystal Structure of *Enterococcus hirae* Enolase at 2.8 Å Resolution

Toshiaki Hosaka[1], Toshiyuki Meguro[1], Ichiro Yamato[1,*] and Yasuo Shirakihara[2]

[1]Department of Biological Science and Technology, Tokyo University of Science, 2641 Yamazaki, Noda-shi, Chiba 278-8510; [2]Laboratory of Biomolecular Structure, National Institute of Genetics, Yata 1111, Mishima-city, Sizuoka 411-8540

Received February 4, 2003; accepted April 14, 2003

We report the crystal structure of an enolase from *Enterococcus hirae*, which is the first report of a structure determination among gram-positive bacteria. We isolated the enolase gene and determined the base sequence. The amino acid sequence deduced from the DNA sequence suggests that this enolase is composed of 431 amino acids. The amino acid sequence is very similar to those of enolases from eukaryotic and prokaryotic organisms, being 65% and 50% identical to enolases from *Escherichia coli* and yeast, respectively. The enolase prepared from *E. hirae* lysate yielded crystals containing one dimer per asymmetric unit. X-ray diffraction patterns were obtained at 2.8 Å resolution on a SPring-8 synchrotron radiation source. Crystals belong to space group *I*4 with unit cell dimensions of $a = b = 153.5$ Å, $c = 90.7$ Å. The *E. hirae*, yeast, *E. coli* and lobster enolase structures are very similar. The *E. hirae* enolase takes an "Open" conformation. The regions in the structure that differ most from other enolases are loops L4 (132–140) and L3 (244–265). Considering the positions of these loops relative to the active site, they seem to have no direct involvement in function. Our findings show that the three dimensional structure of an important enzyme in the glycolytic pathway is evolutionarily conserved among eukaryotes and prokaryotes, including gram-positive bacteria.

Key words: enolase, *Enterococcus hirae*, glycolytic pathway, gram-positive bacteria, recrystallization, X-ray structure.

Abbreviations: PGA, D-(+)-2-phosphoglyceric acid; PEP, phosphoenolpyruvate; EDTA, ethylenediaminetetraacetate; TOF-MS, time-of-flight mass spectroscopy.

Enolase (2-phospho-D-glycerate hydrolyase, EC 4.2.1.11) is a "metal-activated metalloenzyme" (*1*) that catalyses the reversible dehydration of D-(+)-2-phosphoglyceric acid (PGA) to phosphoenolpyruvate (PEP) as a composite reaction of glycolysis and gluconeogenesis (*2*). Enolases from various organisms comprise dimers with two identical subunits (*3*, *4*). Enolase shows an absolute requirement for certain divalent metal ions for activity. The natural cofactor is Mg^{2+}, which gives the highest activity (*5*, *6*). Two types of metal binding sites, site I and site II, contribute to the catalysis (*7*). Metal binding at site I, traditionally called the "conformational" site, induces a conformational change in the active site and enables binding of substrate or substrate analogues. The metal ion bound at this site is difficult to eliminate without the use of high chelator concentrations. The second metal ion, called the "catalytic" metal ion, is bound at site II (*8*, *9*) and its binding induces the catalytic reaction (*7*).

The structure of an enolase from yeast was first reported by Lebioda and coworkers (*10–12*). Duquerroy *et al*. investigated the structure of the enolase from lobster (*13*) and Karin and Ben the enolase from *E. coli* (*14*). The structures of apoenolase (*12*) and various substrate complexes, such as enolase-Mg^{2+} (*15*), enolase-Mg^{2+}-PGA (*16*), enolase-PGA-2Mg^{2+} (*17*), enolase-Mg^{2+}-PGA/PEP (*16*) and so on, are available, in addition to those of a series of inhibitor complexes.

Recent high-resolution structural data on enolase-substrate complexes have made it possible to correlate the structure with the enzymatic characteristics of enolase and various site-specific mutants (*18*). The enzymatic reaction is suggested to involve the stepwise dehydration of 2-phosphoglycerate (*19*, *20*) through an *anti* β-elimination mechanism (21; Scheme 1). In the first step, a base abstracts the proton from C2 of 2-phosphoglycerate, forming a carbanion. In the second step, the hydroxyl group at C3 is eliminated by general-acid catalysis of the carboxyl group of Glu204. Lys345 and Glu211 in yeast enolase (*E. hirae*: Lys 339 and Glu204, respectively) have been proposed to act as a catalytic base-acid pair (*17*, *18*). An alternative proposal suggests that Glu211 and Glu168 in yeast enolase share a proton, which then catalyzes the abstraction of the hydroxyl group (*14*, *16*).

Enolase exists universally among living organisms from mycoplasma to human. The alignments of the amino acid sequences and the structures of these enolases show them to be very similar (Fig. 1). Thus enolase is considered to be evolutionarily conserved because the enzyme is concerned with the glycolytic and glyconeogenetic pathways and is a universally important protein. The structures of enolases from a higher eukaryotic organism, lobster, a lower eukaryotic organism, yeast, and a gram-negative bacterium, *E. coli*, have been elucidated up to now, however, the structures of gram-positive bacterial

*To whom correspondence should be addressed: Tel: +81-4-7124-1501, ex 4405, Fax: +81-4-7125-1841, E-mail, iyamato@rs.noda.tus.ac.jp.

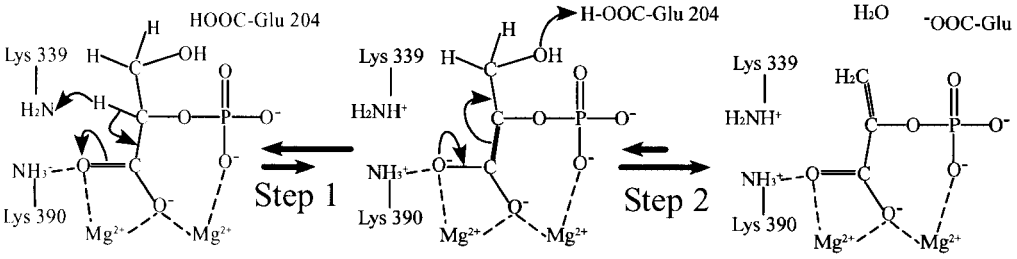

Scheme 1.

and archaebacterial enolases have not yet been determined. In consideration of the conservation of this enzyme throughout evolution, it is important to compare the structures from various organisms. Here, we present the first report of the X- ray structure of an enolase from a gram-positive bacterium, *E. hirae*.

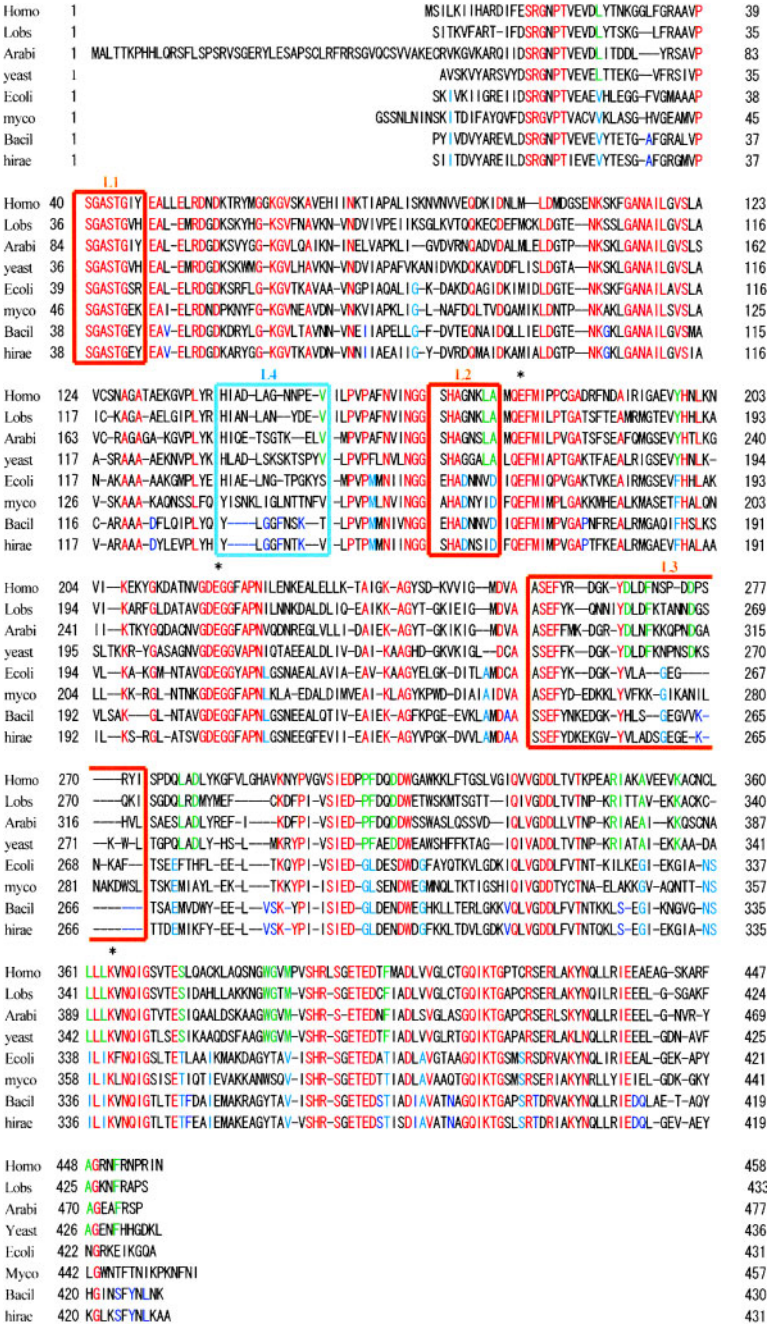

Fig. 1. **Alignment of the amino acid sequence of *E. hirae* enolase with those of other enolases.** Numbers at the ends of each line are those of amino acid residues of different enolases starting from the amino termini. Alignment of the amino acid sequence of the *E. hirae* (hirae) enolase with those of the *Homo sapiens* lung-specific α enolase (Homo), *Homarus gammarus* (Lobs), *Arabidopsis thaliana* (Arabi), *Saccaromyces cerevisiae* (yeast), *E. coli* (Ecoli), *Mycoplasma genitalium* (myco), and *Bacillus subtilis* (Bacil) enolases is shown. Identical residues are coloured as follows: red indicates residues that are identical in all, blue indicates residues that are identical in gram-positive bacteria, green indicates residues that are identical in eukaryotes and cyan indicates residues that are identical in prokaryotes. L1, L2, L3, and L4 indicate loop1, loop2, loop3, and loop4, respectively. *Asterisks* indicate important residues for catalysis.

EXPERIMENTAL PROCEDURES

Amplification and Sequencing of E. hirae Enolase DNA—Genomic DNA was extracted from *E. hirae* (ATCC9790) (*22*). PCR primers were designed by refering to the *E. feacalis* enolase gene (THE INSTITUTE FOR GENOMIC RESEARCH, Gene page: EF1961) that is closely related to *E. hirae.* The primers were (N-term) 5′-ATG TCA ATY ATY ACT GAY GTN TAY GCA CGC GAA-3′ and (C-term) 5′-AGC ATC CAA GAA GCA CCC AT-3′, where Y stands for pyrimidine and N for any base. *E. hirae* DNA was subjected to PCR amplification with these primers. The DNA sequence of the amplified enolase gene was directly determined by dideoxy sequencing (*23*).

Amino Acid Sequencing of E. hirae Enolase—The N-terminal amino acid sequence of the enolase was analyzed by Takara Shuzo (Shiga).

Culture of E. hirae—E. hirae cells were cultured at 37°C in KTY medium for 9 hours (*24*), washed, and disrupted using a French press as described previously (*24*). The cell lysate was obtained after centrifugation at 20,000 ×*g* for 15 min at 4°C after disruption.

Purification of Enolase—Streptomycin sulfate was added to 1% saturation to the cell lysate. The solution was stirred for 30 min at 4°C and then centrifuged at 20,000 ×*g* for 30 min at 4°C. Ammonium sulfate was further added to the supernatant to 40% saturation. The solution was stirred for 1 h at 4°C and then centrifuged at 20,000 ×*g* for 30 min at 4°C. Ammonium sulfate was added to the supernatant to 75% saturation to precipitate enolase. The 75% ammonium sulfate pellet obtained was resuspended in distilled water and dialyzed against 3 liters of buffer A [20 mM MES-Tris (pH6.0), 10% glycerol, 5 mM $MgSO_4$, 1 mM dithiothreitol (DTT), 100 mM KCl] for 12 h at 4°C.

The dialyzed sample was loaded onto a Q-column (Bio-Scale Q20, BIO-RAD; column size, 15 × 113 mm) equilibrated at room temperature with buffer A. The enzyme was eluted with a linear gradient of 0 to 700 mM KCl in the same buffer. The enolase fractions were dialyzed against 3 liters of buffer B [5 mM Tris-HCl (pH 7.5), 100 mM KCl, 10% glycerol, 1 mM DTT, 5 mM $MgSO_4$] for 12 h at 4°C. The sample was loaded onto a Q-column equilibrated at room temperature with buffer C [20 mM Tris-HCl (pH 7.5), 10% glycerol, 5 mM $MgSO_4$, 100 mM KCl, 1 mM DTT] and eluted with a linear gradient of 100 to 700 mM KCl in the same buffer. The enolase fractions were concentrated to 1 ml and the sample was loaded onto a gel filtration column (Superose 6HR; Amersham Biosciences; column size, 20×500 mm) equilibrated with buffer D [20 mM Tris-HCl (pH 7.5), 10% glycerol, 5 mM $MgSO_4$, 50 mM KCl, 2 mM DTT] and eluted with the same buffer.

Enolase Assay—Enzyme activity was assayed as described by Lee and Nowak (*25*). The assay mixture consisted of 50 mM Tris-HCl (pH 7.5), 2 mM PGA, 1 mM $MgCl_2$, 50 mM KCl, and 0.01 mM EDTA in 1 ml and the reaction was performed at room temperature. The increase in absorbance at either 230 or 240 nm was measured. The arbitrary specific activity was defined as the change in absorbance at 240 nm/min or at 230 nm/min divided by enzyme concentration expressed as absorbance at 280 nm (*26*). The kinetic data are reported as specific activity in standard activity units (micromoles of product per minute per milligram = units per milligram). One unit of our arbitrary activity measured at 230 nm [$(\Delta A_{230}/A_{280})$ min^{-1}] corresponds to 0.32 unit/mg and one unit of activity measured at 240 nm [$(\Delta A_{240}/A_{280})$ min^{-1}] corresponds to 0.576 unit/mg. The specific activity of pure yeast enolase at pH 7.5 is 330 $(\Delta A_{230}/A_{280})$ min^{-1} at 30°C or 124 units/mg at 22°C (*27*). Protein was assayed by the method of Lowry *et al*. (*28*) with bovine serum albumin as the standard.

Table 1. **Data collection and refinement statistics.**

Data collection	
space group	*I*4
Unit cell	
$a = b$ (Å)	153.5
c (Å)	90.7
I/sigma (last shell)	7.6 (2.2)
R_{merge} (%) (last shell)	9.3 (34.2)
Completeness (%) (last shell)	100 (100)
Refinement	
Resolution range (Å)	20.0–2.80
R-factor (%)	17.5
Rfree (%)	23.9
Model statistics	
B-factor	($Å^2$)
Average	38.8
main chain	38.1
side chain	39.3
water	35.2
r.m.s.d.[a]	
bond (Å)	0.006
angles (deg.)	1.22
Ramachandran plota	
favored	639
allowed	100
generously allowed	7

[a]Values determined using CNS (*32*) and PROCHECK (*35*), respectively.

Crystal Growth and Recrystallization—Twenty mg/ml enolase was equilibrated at 5°C by the hanging drop method in Tris buffer (100 mM, pH 7.5), 25–30% PEG4000 and 0.2 M Li_2SO_4. We obtained crystals (0.2 × 0.2 × 0.03 mm) comprising more than 7 dimers per asymmetric unit. These crystals were them dissolved in buffer D and the protein was recrystallized under the same conditions. Protein concentrations were between 5 and 8 mg/ml. Crystals, approximately 0.1 × 0.1 × 0.1 mm, were obtained in 3–5 days.

X-Ray Data Collection and Processing—Diffraction data were collected at 100 K with a MARCCD detector at SPring-8 BL41-XU beamline and the wavelength was set to 1.0 Å. The data were processed with MOSFLM (*29*) and the CCP4 suite (*30*). The crystals belonged to space group *I*4 and had unit cell dimensions of $a = b = 153.5$ Å and $c = 90.7$ Å. The crystals contained one dimer per asymmetric unit ($V_M = 2.86$ $Å^3$/Da) and diffracted to 2.80 Å resolution. A summary of the data collection statistics is given in Table 1.

Molecular Replacement—The molecular structure of the enolase was solved by molecular replacement with the Molrep software (*31*) programs of the CCP4 suite,

Table 2. **Purification table.**

Purification step	protein (mg)[a]	protein (mg)[b]	sp. ac.[c] (units/mg)	total units[c]	purification factor[c]	A_{280}/A_{260}
streptomycin fractionation	5,387	(2,585)	2.57	13,845	1.0	0.52
$(NH_4)_2SO_4$ fractionation	3,510	(1,260)	2.31	8,108	0.90	0.68
Q column (pH 6.0)	771	(90.3)	6.60	5,089	2.57	0.45
Q column (pH 7.5)	344	(33.3)	11.4	3,922	4.44	0.45
gel filtration	108	(27.3)	27.9	3,073	10.9	0.55
recrystalization	N. D.[d]		162	N. D.[d]	65.6	1.77

[a,b]Protein was estimated using A_{280} and measured by the method of Lowry *et al.* (*28*), respectively. [c]Values were represented by using the protein content estimated by A_{280}. [d]Not determined.

using a yeast enolase dimer as a search model (1EBH) (*15*). One dimer was placed in the asymmetric unit. Iterative cycles of rigid body refinement, simulated annealing, individual *B*-factor refinement with CNS (*32*) and solvent flattening with DM (*33*) were carried out. XtalView (*34*) was used to inspect the electron density maps, models and the manual rebuilding of the model structure. After the first three cycles of refinement, the yeast residues were mutated to the corresponding *E. hirae* residues. Then cycles of simulated annealing, energy minimization and *B*-factor refinement with CNS and model rebuilding were repeated. Water molecules were placed automatically with CNS. Water and glycerol molecules were placed manually with XtalView at positive peaks of the difference map $|F_O|-|F_c|$. In total, 176 water molecules were introduced into the model. The final *R*-factor was 17.5% and the R_{free} 23.9%.

Structure validation was done with PROCHECK (*35*): 85.7% of residues were in the core region of the Ramachandran plot, 13.4% in the allowed regions, 0.9% in the generously allowed regions and no residues in the disallowed region.

RESULTS AND DISCUSSION

The Sequence of E. hirae Enolase—The amino acid sequence of *E. hirae* enolase was deduced from the DNA sequence of the PCR-amplified DNA fragment. We identified the open reading frame (ORF) composed of 431 amino acids. Residues 1–22, which were determined by N-terminal amino acid sequencing, were identical to the deduced amino acid sequence. The ORF was compared with other known enolase sequences, showing that all enolases, including those from eukaryotes and prokaryotes, are highly homologous (Fig. 1). *E. hirae* enolase is 50% and 65% identical to yeast and *E. coli* enolases, respectively (Fig. 1). *E. hirae* and *Mycoplasma genitalium* enolases share 54% sequence identity. We concluded that the primary sequence of enolase has remained conserved throughout evolution. Loops L1 (38–45), L2 (152–159), and L3 (244–265) have been defined as catalytic loops in previous reports on structure and function (*14*). Therefore, we defined loop L4 (132–140) additionally, as a unique loop in enolases from gram-positive bacteria (Fig. 1, Bacil & hirae).

Purification and Crystallization of Enolase—Ammonium sulfate fractionation was performed followed by chromatography on a Q-column and gel filtration. This procedure yielded enolase with a specific activity of 27.9 arbitrary units/mg at 22.1% yield. The purification process is summarized in Table 2.

After recrystallization, we obtained adequate diffraction data. By recrystallization, the A_{280}/A_{260} value of the protein solution increased from 0.55 to 1.77, so it appears that recrystallization was effective for purification increasing the quality of the crystals (Table 2). Correspondingly, the specific activity increased to 162 arbitrary units/mg (Table 2), which is comparable to the value obtained for yeast enolase (*25*). The resuspended solution was analysed by TOF-MS and a molecular weight of 46,623.5 was determined. This molecular weight is almost identical to that calculated from the amino acid sequence (46,220 Da).

Overall Structure—Crystals contained one dimer per asymmetric unit (V_M = 2.86 Å^3/Da) and diffracted to 2.80 Å resolution. A summary of the data collection statistics and refinement results is given in Table 1. The overall structure of the homodimer enolase comprised of all 431 amino acids was determined (Fig. 2). Presently, 176 water molecules (temperature factors < 66 Å^2), two SO_4^{2-} and Mg^{2+} around the active sites have been identified in the dimeric model. Additionally, we identified 6 glycerol molecules around the dimer surface, since we used glycerol as cryoprotectant. Glycerol molecules were placed manually with XtalView at positive peaks of the difference map $|F_o|-|F_c|$. At first, three or four water molecules were placed at each position. But, these water molecules were so closely located that they repelled each other by simulated annealing. Therefore, we believe that these peaks correspond to glycerol molecules.

This structure shows the identical secondary structure of members of the enolase superfamily. One subunit of enolase showed two domains. The N-terminal domain comprised residues 1–133 and consisted of a three-

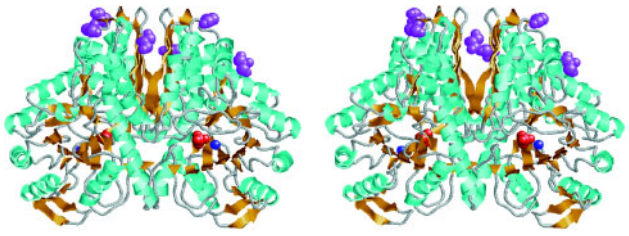

Fig. 2. **Stereo view of the *E. hirae* enolase dimer.** The dyad axis is oriented vertically. The glycerol molecules are coloured in magenta, the Mg^{2+} ions are in blue and the SO_4^{2-} ions are in red. The rendered protein model was made with Rasmol (*39*).

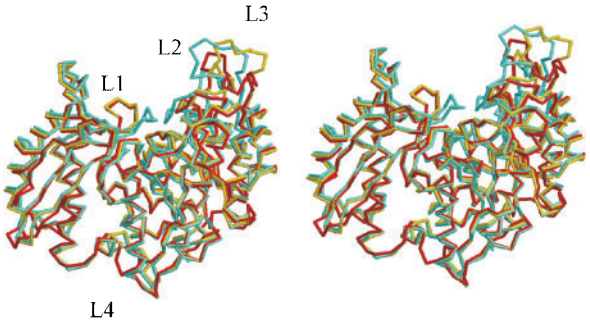

Fig. 3. **Stereo view of *E. hirae* and yeast enolases.** Comparison of the enolase structure of *E. hirae* (red) with those of yeast (cyan, 2ONE; yellow, 1EBH) enolases is shown. Mobile loops are labeled. Superpositions of the Cα atom coordinates of the *E. hirae* enolase and respective enolases of "Closed" type (cyan) and "Open" type (yellow) are indicated.

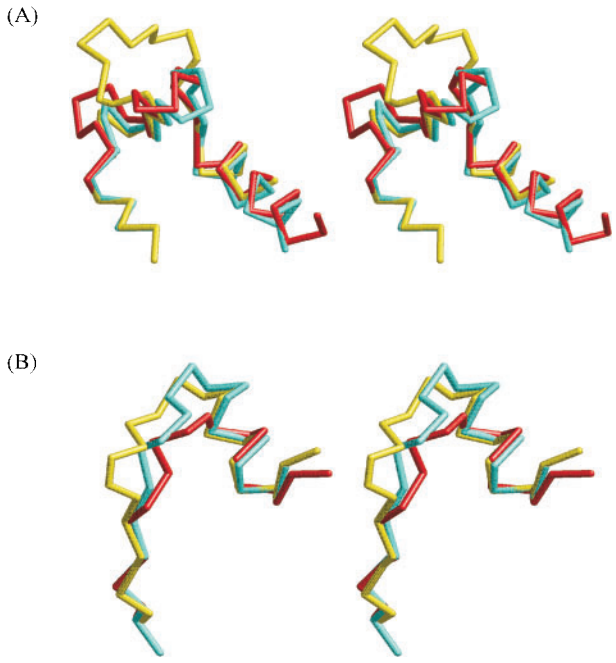

Fig. 4. **Stereo views of the L3 and L4 regions.** Comparisons of *E. hirae* (red), *E. coli* (cyan; 1E9I: subunit A) and yeast (yellow; 1EBH) "Open" enolase L3 and L4 regions are shown. Superposition was done with "Databases and Tools for 3-D Protein Structure Comparison and Alignment" (*40*). (A) L3 region. (B) L4 region.

stranded antiparallel β-sheet followed by four α-helices. The C-terminal domain consisted of an eight-stranded mixed α/β-barrel with the connectivity $\beta\beta\alpha\alpha(\beta\alpha)_6$. These domains were connected through L4 (Figs. 1 and 3). Like other members of the triose-phosphate isomerase (TIM) barrel architecture family (*36*), the principal enolase domain showed an 8-fold barrel. However, it deviated somewhat from the simpler $(\beta\alpha)_8$ topology of the TIM barrel and had an unusual $\beta\beta\alpha\alpha(\beta\alpha)_6$ organization (*11*, *36*).

The electron density was very well refined except for parts of the surface and loops. Especially, poorly ordered regions of the atomic model (loops L1, L2, and L3, which are movable toward the active center) were omitted at the initial stages of refinement. In these regions, the correlations between the observed and calculated electron densities remained lower than average and main-chain isotropic temperature factors were higher than average even after refinement. All residues in the main chain were well-defined except residues 41–43 in both subunits and residues 152 and 252 in subunit B. Also, the side chain densities at the surface of subunit B were less clear and indicated some disorder.

The average values of temperature factors for all atoms in subunits A and B were 34.5 and 41.4 Å^2, respectively. The higher B-factor region was found around L3 of subunit B. Because the contact between molecules is loose at this region, the structure may be disordered. It was difficult to distinguish the water molecules and side chains of L3 around this region.

The structures of *E.hirae*, lobster, yeast (1EBH, 2ONE) (*15*, *16*) and *E. coli* [1E9I (A), (D)] (*14*) enolases are very similar. The root-mean-square distance (r.m.s.d.) between Cα positions in two subunits of *E. hirae* enolase is 0.61 Å. The r.m.s.d.'s of Cα atom positions in both subunits are 1.1 Å and 1.4 Å by comparing the *E. hirae* enolase with yeast enolase "Open" type (1EBH) and yeast enolase "Closed" type (2ONE) that binds the substrate, respectively (Fig. 3). Also, the r.m.s.d.'s of Cα atom positions are 0.9 Å and 1.4 Å by matching the *E. hirae* enolase with *E. coli* enolase "Open" type (1E9I subunit A) and *E. coli* enolase "Closed" type (1E9I subunit D), respectively. The L1, L2 and L3 regions of the "Open" conformation shift largely towards the active site in the "Closed" conformation with bound substrate. Considering the positions of these three loops, we believe that the structure of *E. hirae* enolase corresponds to the "Open" conformation (*14*, *16*).

L3 and L4 Regions—The primary to tertiary structures of prokaryotic and eukaryotic enolases are fairly conserved (Figs. 1 and 3), suggesting strong evolutionary conservative pressure. The largest differences between the prokaryotic and eukaryotic enolases are at loops L3 (244–265) and L4 (133–139).

The L3 loops of *E. hirae* and *E. coli* (*E. coli*: 248–267) enolases are 5 residues shorter than yeast enolase (yeast: 249–273) (Fig. 1) (*16*, *37*). Compared to animal enolases, this L3 loop is on average four residues shorter in prokaryotic enolases and 2 residues longer in plant enolases (*16*, *37*). The L3 loops of prokaryotic enolases from *E. hirae* and *E. coli* show anti-parallel β-sheets, while those of eukaryotic enzymes from yeast and lobster have more flexible structures (Fig. 4A) (*14–16*). The region moves towards the active site upon substrate binding (Figs. 3 and 4A) (*14–17*). However, the differences in the L3 structures do not seem to affect enzyme activity. Thus we do not think that the L3 region plays an important functional role.

The L4 loop connects the N-terminal domain and barrel domain. In comparison with other enolases, the L4 loop of the gram-positive bacterial enolase seems to have a unique amino acid sequence and structure (Figs. 1 and 4B). Characteristic amino acids in L4 loop of enolase from gram-positive bacteria accounted for up to 21.2% of the characteristic amino acids commonly found in the whole amino acid sequences of enolases from gram-positive bacteria (Fig. 1, blue letters). The L4 loops of enolases from gram-positive bacteria, *E. hirae* and *Bacillus subtilis*, are

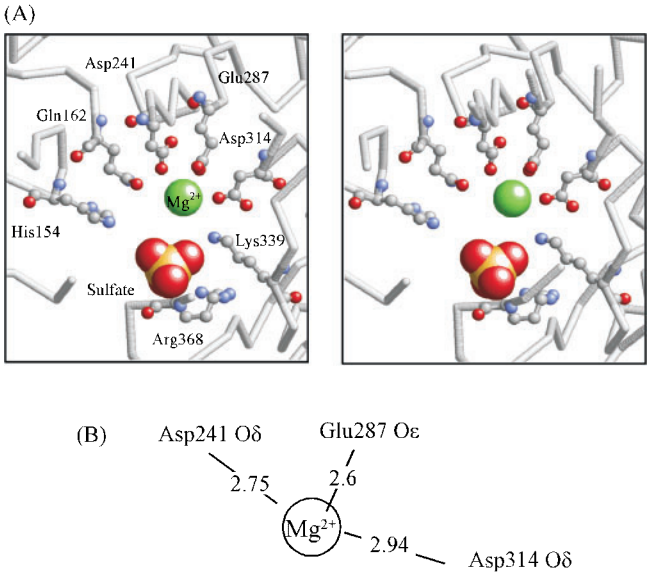

Fig. 5. **(A) Structure at the active site of the *E. hirae* enolase with the sulfate and magnesium ions.** The rendered protein model was made with Rasmol (*39*). (B) Schematic representation of the environment of the Mg^{2+} at the active site of enolase. The distances are shown in angstroms.

shorter than those from animals, plants and gram-negative bacteria (Figs. 1 and 4B). Correspondingly, the average temperature factor at this loop (21.3 Å^2) is lower than other regions in the enolase (L4/all regions: 0.55). This shorter L4 loop in *E. hirae* may cause a tighter connection of the N-terminal and barrel domains, which in turn may have some relevance to structural stability. In this respect, an investigation of heat stability and/or protease sensitivity of various enolases is required. However, since the L4 loop resides far away from the active site (about 28 Å), we do not think that the difference in this region is of catalytic significance.

The highly conserved primary sequences of enolases among various organisms indicate the biological importance of enolase in the universal metabolic pathway. Our study of the three dimensional structure of an enolase from a gram-positive bacterium, *E. hirae*, reinforces this view: the three dimensional structures are also highly conserved among various organisms. In this respect, the structure determination of an enolase from an Archaebacterium is awaited.

The Active Site—The active sites of *E. hirae*, yeast, lobster and *E. coli* enolases show very similar primary structural features (Fig. 1). All residues involved in catalysis (Glu163, Glu204, Lys339) are well conserved (Figs. 1 and 5).

Two magnesium ions per subunit are required for catalytic activity (*7*). The second magnesium ion is bound with lower affinity after the substrate is bound (*8*, *9*). The *E. hirae* enolase structure corresponds to the "Open" conformation (Fig. 3), therefore, one magnesium ion should be detected in the electron density map. We identified the magnesium ion surrounded by Asp241, Glu287 and Asp314 (Fig. 5). We also identified one water molecule near the magnesium ion, although in yeast enolase (1EBH) three water molecules near the magnesium ion were identified (*15*). The resolution of our sample was not sufficient to distinguish such electron density in this region.

The *E. hirae* enzyme also shows high electron density at the position corresponding to the phospho group in the yeast enolase complex with 2-phospho-D-glycerate (G2P) and phosphoenolpyruvate or with an intermediate analogue (*15*, *17*). In the substrate-free forms of both yeast and lobster enolases, sulfate ions have been found at the corresponding position (*12*, *13*). In the *E. hirae* enolase structure (Fig. 5), we attributed the high electron density to a sulfate ion, because the solution for crystallization contained 0.2 M Li_2SO_4 and 2.5 mM $MgSO_4$.

The Dimer Interface—Precise analysis of the *E. hirae* enolase dimer interface with the 'Protein-Protein Interaction Server' (*38*) showed that the enolase dimer interface is more planar than the average homodimer interface. The *E. hirae* enolase subunit contact in the dimer had a burial of surface of 3148.5 Å^2, which is similar to the average buried surface of 3370 Å^2 found for other homodimeric proteins (*38*). The dimer interface of *E. coli* and yeast enolases also have similar surface burials of 3332.7 Å^2 and 3575.9 Å^2, respectively (*14*). The value for the interface planarity, defined as the r.m.s.d. of the interface atoms from the best fit plane through the interface, is 1.8 Å in the *E. hirae* enolase dimer as compared to an average value of 3.5 Å. The enzyme shows no known cooperative effect, so the interface does not seem to have any allosteric function.

In both subunits, the dihedral angles assigned to Arg396 lie in the generously allowed regions of the Ramachandran plot. This residue was omitted prior to refinement and the electron density map was calculated. Therefore, this position is not model biased. Arg396 resides at the dimer interface and connects the last strand with the helix of the barrel domain. The CO atom of Arg396 forms hydrogen bonds with the amide nitrogen atoms of Arg399 and Ile400. Additionally, the NH atom of Arg396 forms hydrogen bonds with the OD1 and OD2 atoms of Asp398 and with the CO atom of Ser14. Interestingly, the residues corresponding to Arg396 in *E. coli* enolase (Arg398), yeast enolase (Arg402), and lobster enolase (Arg401) are all in the generously allowed regions (*14*). The residue is retained by interactions with the environment in a stressed state that stabilizes the dimer structure.

We thank Dr. Masahide Kawamoto of JASRI for valuable help with data collection using synchrotron radiation of BL41XU, SPring-8. The atomic coordinates for *E. hirae* enolase have been deposited in the Protein Data Bank as entry 1IYX. The DNA sequence of the *E. hirae eno* gene is available from the GenBank/EMBL/DDBJ databases under accession number AB091345.

REFERENCES

1. Brewer, J.M. (1981) Yeast enolase: mechanism of activation by metal ions. *CRC Crit. Rev. Biochem.* **11**, 209–254
2. Wold, F. (1971) in The Enzymes (Boyer, P.D., ed.) Vol. **5**, 3rd ed., pp. 499–538, Academic Press, New York
3. Brewer, J.M. and Weber, G. (1968) The reversible dissociation of yeast enolase. *Proc. Natl Acad. Sci. USA* **59**, 216–223

4. Brewer, J.M., Fairwell, T., Travis, J., and Lovins, R.E. (1970) An investigation of the subunit structure of yeast enolase. *Biochemistry* **9**, 1011–1016
5. Wold, F. and Ballou, C.E. (1957) Studies on the enzyme enolase II. Kinetic studies. *J. Biol. Chem.* **227**, 313–328
6. Brewer, J.M. (1985) Specificity and mechanism of action of metal ions in yeast enolase. *FEBS Lett.* **182**, 8–14
7. Faller, L.D., Baroudy, B.M., Johnson, A.M., and Ewall, R.X. (1977) Magnesium ion requirements for yeast enolase activity. *Biochemistry* **16**, 3864–3869
8. Hanlon, D.P. and Westhead, E.W. (1969) Kinetic studies on the activation of yeast enolase by divalent cations. *Biochemistry* **8**, 4255–4260
9. Brewer, J.M. (1971) The increase of yeast enolase fluorescence produced by substrates and competitive inhibitors in the presence of excess Mg^{2+}. *Biochim. Biophys Acta* **250**, 251–257
10. Lebioda, L. and Stec, B. (1988) Crystal structure of enolase indicates that enolase and pyruvate kinase evolved from a common ancestor. *Nature* **333**, 683–686
11. Lebioda, L., Stec, B., and Brewer, J.M. (1989) The structure of yeast enolase at 2.25-Å resolution. An 8-fold β + α-barrel with a novel ββαα $(\beta\alpha)_6$ topology. *J. Biol. Chem.* **264**, 3685–3693
12. Stec, B. and Lebioda, L. (1990) Refined structure of yeast apoenolase at 2.25 Å resolution. *J. Mol. Biol.* **211**, 235–248
13. Duquerroy, S., Camus, S., and Janin, J. (1995) X-ray structure and catalytic mechanism of lobster enolase. *Biochemistry* **34**, 12513–12523
14. Kuhnel, K. and Luisi, B.F. (2001) Crystal structure of the *Escherichia coli* RNA degradosome component enolase. *J. Mol. Biol.* **313**, 583–592
15. Wedekind, J.E., Reed, G.H., and Rayment, I. (1995) Octahedral coordination at the high-affinity metal site in enolase: crystallographic analysis of the Mg^{II}-enzyme complex from yeast at 1.9 Å resolution. *Biochemistry* **34**, 4325–4330
16. Zhang, E., Brewer, J.M., Minor, W., Carreira, L.A., and Lebioda, L. (1997) Mechanism of enolase: the crystal structure of asymmetric dimer enolase-2-phospho-D-glycerate/enolase-phosphoenolpyruvate at 2.0 Å resolution. *Biochemistry* **36**, 12526–12534
17. Larsen, T.M., Wedekind, J.E., Rayment, I., and Reed, G.H. (1996) A carboxylate oxygen of the substrate bridges the magnesium ions at the active site of enolase: structure of the yeast enzyme complexed with the equilibrium mixture of 2-phosphoglycerate and phosphoenolpyruvate at 1.8 Å resolution. *Biochemistry* **35**, 4349–4358
18. Reed, G.H., Poyner, R.R., Larsen, T.M., Wedekind, J.E., and Rayment, I. (1996) Structural and mechanistic studies of enolase. *Curr. Opin. Struct. Biol.* **6**, 736–743
19. Dinovo, E.C. and Boyer, P.D. (1971) Isotopic probes of the enolase reaction mechanism. *J. Biol. Chem.* **246**, 4586–4593
20. Anderson, S.R., Anderson, V.E., and Knowles, J.R. (1994) Primary and secondary kinetic isotope effects as probes of the mechanism of yeast enolase. *Biochemistry* **33**, 10545–10555
21. Cohn, M., Pearson, J.E., O'Connell, E.L., and Rose, I.A. (1970) Nuclear magnetic resonance assignment of the vinyl hydrogens of phosphoenolpyruvate. Stereochemistry of the enolase reaction. *J. Amer. Chem. Soc.* **92**, 4095–4098
22. Marmur, J. (1961) A procedure for the isolation of deoxyribonucleic acid from micro-organisms. *J. Mol. Biol.* **3**, 208–218
23. Sanger, F., Nicklen, S., and Coulson, A.R. (1977) DNA sequencing with chain-terminating inhibitors. *Proc. Natl Acad. Sci. USA* **74**, 5463–5467
24. Kakinuma, Y. and Harold, F.M. (1985) ATP-driven exchange of Na^+ and K^+ ions by *Streptococcus faecalis*. *J. Biol. Chem.* **260**, 2086–2091
25. Lee, M.E. and Nowak T. (1992) Metal ion specificity at the catalytic site of yeast enolase. *Biochemistry* **7**, 2172–2180
26. Westhead, E.W. and McLain, G. (1964) A purification of Brewers' and Bakers' yeast enolase yielding a single active component. *J. Biol. Chem.* **239**, 2464–2468
27. Westhead, E.W. (1966) Enolase from yeast and rabbit muscles. *Methods Enzymol.* **9**, 670–679
28. Lowry, O.H., Rosebrough, N.J., Farr, A.L., and Randall, R.J. (1951) Protein measurement with the Folin phenol reagent. *J. Biol. Chem.* **193**, 265–275
29. Leslie, A.G.W. (1991) in *Crystallographic computing V* (Moras, D., Podjarny, A.D., and Thierry, J.C., eds.) pp. 27–38, Oxford University Press, Oxford
30. Collaborative Computational Project, Number 4 (1994) The CCP4 suite: programs for protein crystallography. *Acta Crystallogr.* **D50**, 760–763
31. Vagin, A. and Teplyakov A. (1997) MOLREP: an automated program for molecular replacement. *J. Appl. Crystallogr.* **30**, 1022–1025
32. Bruger, A.T., Adams, P.D., Clore, G.M., DeLano, W.L., Gros, P., Grosse-Kunstleve, R.W. *et al*. (1998) Crystallography & NMR system: a new software suite for macromolecular structure determination. *Acta Crystallog. Sect. D* **54**, 905–921
33. Cowtan, K. and Main, P. (1998) Miscellaneous algorithms for density modification. *Acta Crystallog. Sect. D* **54**, 487–493
34. McRee, D.E. (1999) XtalView/Xfit–A versatile program for manipulating atomic coordinates and electron density. *J. Struct. Biol.* **125**, 156–165
35. Laskowski, R.A., MacArthur, M.W., Moss, D.S., and Thornton, J.M. (1993) PROCHECK: a program to check the stereochemical quality of protein structures. *J. Appl. Crystallog.* **26**, 283–291
36. Banner, D.W., Bloomer, A.C., Petsko, G.A., Phillips, D.C., Pogson, C.I., Wilson, I.A. *et al*. (1975) Structure of chicken muscle triose phosphate isomerase determined crystallographically at 2.5 angstrom resolution using amino acid sequence data. *Nature*, **255**, 609–614
37. Brewer, J.M. and Lebioda, L. (1997) Current perspectives on the mechanism of catalysis by the enzyme enolase. *Adv. Biophys. Chem.* **6**, 111–141
38. Jones, S. and Thornton, J.M. (1996) Principles of protein-protein interactions. *Proc. Natl Acad. Sci. USA* **93**, 13–20
39. Sayle, R.A. and Milner-White, E.J. (1995) RASMOL: biomolecular graphics for all. *Trends Biochem. Sci.* **20**, 373–375
40. Shindyalov, I.N. and Bourne, P.E. (1998) Protein structure alignment by incremental combinatorial extension (CE) of the optimal path. *Protein Eng.* **11**, 739–747